CrossMark

TECHNICAL PAPER

Bulk silicon micromachined suspended fixed-end SiO₂ film capacitor for passive high-pass RC filter

Jianxiong Zhu[1] · Hua Zhu[2]

Abstract We reported a suspended fixed-end 5 μm thin SiO₂ film beam and plate MEMS capacitor for passive high-pass RC filter. This suspended structure was fabricated using bulk silicon two-sided alignment micromachining technology. The dynamic model included both a first order derivative of a high-pass filter electrical system and MEMS variable capacitors driven by electrostatic force. The room temperature experiment showed that the MEMS high-pass filter circuit can convert a rectangular wave input signal into high frequency spikes at its output. Finite element calculating software *COMSOL* and numerical simulation *MATLAB* were both used to evaluate the motion modal and the output voltage. Compared with the commercial static capacitor in a high-pass filter, we could also find that the coupling of the electrostatic force and dynamic motion of the electrode plate in the designed single device and dual-device could show an asymmetric offset voltage electrical response.

1 Introduction

Micro-electro-mechanical system (MEMS) filter has received significant attention due to their fascinating functional application in robotics, sensors, energy harvester, signal processing system in loudspeaker and micro-communication (Bijari et al. 2012; Chivukula and Rhoads

2010; Hore et al. 2016; Lang et al. 2011; Saha et al. 2011; Wang et al. 2010). A low-pass or high-pass filter is an electronic filter that passes signals with a frequency lower or higher than a certain cutoff frequency. And capacitor takes a key factor of the frequency cutoff in the filter (Saha et al. 2011; Wang et al. 2010). Electrostatically MEMS capacitor not only has the advantage with mechanical dynamic motion and electrical storing for their frequency response (Baginsky et al. 2013; Galayko and Basset 2011; Tvedt et al. 2010), but also has advantage with compact size, simple geometry, low power consumption and ease integration in micro fabrication. Many researchers have reported that MEMS capacitor through electrostatic actuation is highly dependent on parameters, such as actuation forces, squeeze film damping effects, large structural deformation, and intermolecular surface forces (Erbes et al. 2016; Shirazi et al. 2011; Kambali and Pandey 2016; Langfelder et al. 2011; Yang et al. 2010; Zhang et al. 2014). And the behavior of many kinds structural designed filter has also been reported in the literature (Basu and Bhattacharyya 2011; Caruntu and Knecht 2015; Dong et al. 2014; Xu and Cheng 2015; Zhang et al. 2015). Basu and Bhattacharyya 2011 have demonstrated a 2 μm thick polysilicon flexural mode clamped–clamped beam device at a frequency of 10 MHz in vacuum ambient. Xu and Chen2015 have reported in silicon extensional mode device vibrating at 2.18 MHz using square plates operating in the bulk mode of vibration. However, all the researches were focused on the extremely high frequency in resonator. Almost no group has carried out the research about the variable MEMS capacitor with beam and plate structural application in high-pass RC filter, especially the frequency around 1 kHz. We have taken the research about a suspended fixed-end thin SiO₂ film beam and plate as high-pass RC filter for the frequency range 300–2500 Hz, and we also found an asymmetric offset

✉ Jianxiong Zhu
  zhujianxiong@binn.cas.cn

[1] Beijing Institute of Nanoenergy and Nanosystems, Chinese Academy of Sciences, Beijing 100083, China

[2] Department of Mechanical and Aerospace Engineering, University of Missouri Columbia, Missouri 65211, USA

voltage electrical response because of the coupling of the electrostatic force and dynamic motion of the electrode plate in the variable MEMS capacitor.

2 Design and modeling

The suspended fixed-end variable beam and plate capacitor shown in Fig. 1a, b was designed with bulk silicon micromachined technology. The proof-mass movable 5 μm thickness SiO$_2$ film was supported by two fixed-end SiO$_2$ suspension beams. The top surface of the SiO$_2$ film was sputtered Cu by megnetron sputtering (*PVD 75 Pro Line Kurt J. Lesker Company*) for 5 min and the bottom fixed square plate on the silicon substrate was patterned with chromium (Cr) 1 min and gold (Au) 2 min by megnetron sputtering equipment as well. Both the suspended SiO$_2$ film plate and the bottom gold square plate formed a variable capacitor. When a rectangular wave signal imposed onto this variable capacitor shown in Fig. 1c, the movable plate motions due to the changeable electrostatic force interaction with the bottom gold fixed plate. When a variable capacitor and output test resistor is connected to a circuit with direct current (DC) source, two processes related the capacitor, which are called "charging" and "discharging" the capacitor, will happen due to the energy storing of the capacitor in its electric field. And both plates get the equal and opposite charges, and an increasing potential difference is created while the capacitor is charging. Once the voltage at the terminals of the capacitor and the output resistor is equal to the power supply voltage V_{in}, the capacitor is fully charged and the transient current stops flowing. Notice that the transient currents decay and the time in the designed circuit depend on the resistance (R_{out}) and capacitance (C).

When the capacitive filter is subjected with a rectangular wave, the arrival of the falling edge of the input waveform causes the variable capacitor to reverse charge giving a negative output spike, then as the square wave input changes during the output spike changes from a positive value to a negative value. As shown in Fig. 1c, the initial separation between the two plates, d_0, is used as the characteristic length throughout of this paper. The variable x is the dimensionless displacement of the movable plate from the equilibrium. Parameter $C(t)$ is the variable capacitor, C_p represents the parasitic capacitance related to the variable capacitor, C_{in} represents the input capacitance of the voltage measurement circuit which is directly related with the measured voltage. Since the effect of C_p can be lumped into $C(t)$, we assume that $C_p = 0$ is without loss of generality. The charge on $C(t)$ shown in Fig. 1d is given by
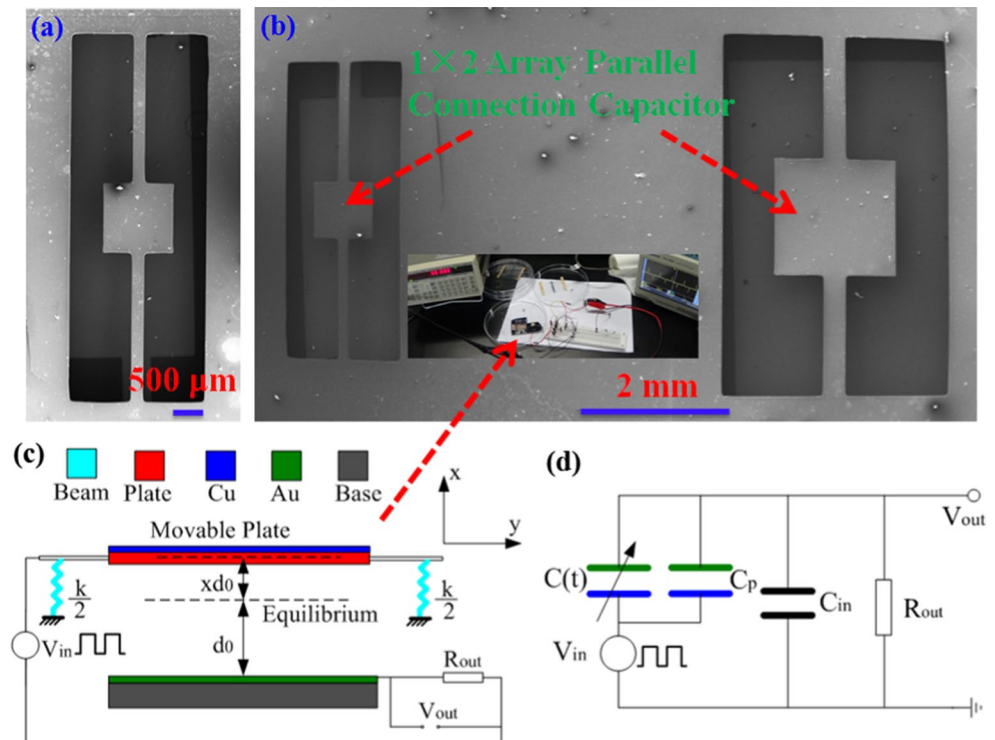
$$Q = C(t)(V_{in} - V_{out}), \tag{1}$$

the derivative on both side of equation is as follows,

$$\dot{Q} = \dot{C}(t)(V_{in} - V_{out}) - C(t)\dot{V}_{out}. \tag{2}$$

It knows that the charge over C_{in} is given by

$$Q_1 = C_{in}V_{out}. \tag{3}$$

Fig. 1 5 μm thick suspended fixed-end SiO$_2$ film variable capacitive high-pass filter: **a** SEM of a 500 × 500 μm^2 plate and 1 mm × 50 μm supporting beam; **b** SEM of a 1 × 2 array, note the dimension of them are not the same; **c** physical model of MEMS capacitive filter; **d** electrical equivalent model of the variable capacitive RC filter

Based on the Kirchhoff current law in the electrical circuit, we have

$$\dot{Q} = \dot{Q}_1 + \frac{V_{out}}{R_{out}}. \tag{4}$$

Therefore, we get

$$\dot{C}(t)(V_{in} - V_{out}) - C(t)\dot{V}_{out} = C_{in}\dot{V}_{out} + \frac{V_{out}}{R_{out}}. \tag{5}$$

Rearranging the terms in Eq. (5), we finally get

$$R_{out}[C_{in} + C(t)]\dot{V}_{out} + [R_{out}\dot{C}(t) + 1]V_{out} = V_{in}R_{out}\dot{C}(t) \tag{6}$$

which is

$$\dot{V}_{out} = \frac{\dot{C}(t)(V_{in} - V_{out}) - \frac{V_{out}}{R_{out}}}{C_{in} + C(t)}. \tag{7}$$

The parasitic capacitance C_{in} has negligible effect if the capacitive impedance is much larger than R_{out}. The microcantilever and the suspended plate of the MEMS variable capacitive filter are considered as a spring-mass system. The model of the equivalent mass m, spring stiffness k, damping factor b has been extensively explored and modeled (Saha et al. 2011; Galayko and Basset 2011). The electrostatic force between two parallel plates is derived from the following equation,

$$F_e = -\frac{\partial U}{\partial d} \tag{8}$$

where d is the separation of two parallel plates, U is the potential energy given by

$$U = \frac{Q^2}{2C(x)}. \tag{9}$$

The capacitance between two plates can be calculated using the equation,

$$C(x, \theta) = \iint_A \frac{\varepsilon dA}{d}. \tag{10}$$

The movable plate of the variable capacitor is subjected to the nonlinear electrostatic force F_e which is driven by rectangular wave signal, the suspension force from linear springs and the damping force from the air. We follow Newton's second law,

$$m\ddot{x} + c_1\dot{x} + kx = F_e. \tag{11}$$

where c_1 is the viscous damping coefficient added to represent the damping loss. The mechanical and electrical effects are coupling with each other through the motion of the movable plate in the variable capacitive high-pass filter system.

3 Device fabrication

Figure 2 illustrates the fabrication process flow of the variable MEMS capacitor using bulk silicon micromachining technology: (1) a thin SiO_2 was plasma enhanced chemical vapor deposition (PECVD) on a piece of silicon, and then thick photoresist sacrificial layer was coated on this specific SiO_2 (see Fig. 2b). (2) A mask was used during the lithography exposure for the specific structure (see Fig. 2c). (3) Cr and Au was megnetron sputtering deposited (see Fig. 2d), and after this the photoresist sacrificial layer on top of the silicon was removed by carefully flushing with acetone and DI water (see Fig. 2e). (4) A SiO_2 layer with a thickness of 5 μm on the top side and 1 μm SiO_2 film on the back side of a wafer was PECVD grown as well, respectively (see Fig. 2f). (5) A thick photoresist sacrificial layer was coated with a thickness of 15 μm on both side of the wafer for lithography on both side of the water (see Fig. 3g). (6) 5 μm deep SiO_2 and 1 μm SiO_2 were etched away using Inductively Coupled Plasma (ICP) 20 min (see Fig. 3h). Note that a few thickness of silicon etched away. (7) KOH solution was used as bulk wet etching for 48 h (see Fig. 2i). (8) Metallization was carried out by Cr/Au (30/300 nm) which were sputter on the top of the suspended plate and cantilever (see Fig. 2j). (9) Finally, the photoresist sacrificial layer on top of the silicon was removed carefully by flushing with acetone and DI water. (10) Both the two components Fig. 2e and j were boding together to form the variable capacitor (see Fig. 2k).
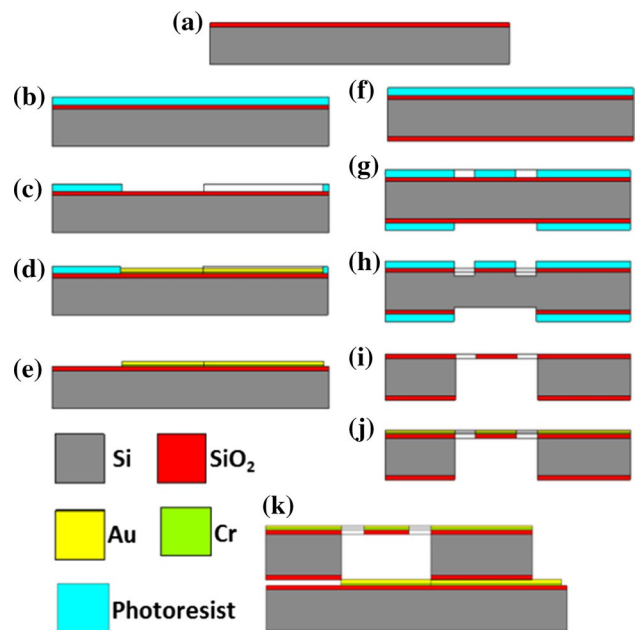

Fig. 2 Fabrication process flow of SiO_2 film fixed-end MEMS variable capacitor

4 Measurement and discussion

Figure 3 illustrates the electrical characteristic performance of the bulk silicon fabricated MEMS variable capacitor using *E4980A Precision LCR*. The 1 × 2 array has 540 pF compared with 500 pF for a single capacitor at frequency 1.2 kHz shown in Fig. 3a. Figure 3b depicts the single cavity has 2 times loss coefficient than the 1 × 2 array. The reason to explain this phenomenon is that the electrostatic force on the variable 1 × 2 array capacitor is much stronger than the single device.

The function generator and an oscilloscope were used to do the experimental test shown in Fig. 4a. The function generator was as an input rectangular wave power source, and the oscilloscope was used to measure the output voltage on the resistors 220 kΩ. Compared with the commercial static capacitor, we found that the stability voltage of capacitor is slightly above zero in MEMS variable device. The coupling effect of the electrostatic force could be used to explain them. When compared with the single device in Fig. 4a and the 1 × 2 array in Fig. 4b, we found that the parallel connection of the 1 × 2 array capacitors with greater value than single capacitor caused better electrical performance. The resonance frequency of the high-pass filter was observed around 1 kHz for both devices (shown in Fig. 4d).

Fig. 3 MEMS variable capacitor with the increasing sweeping frequency: **a** capacitance; **b** loss of the coefficient
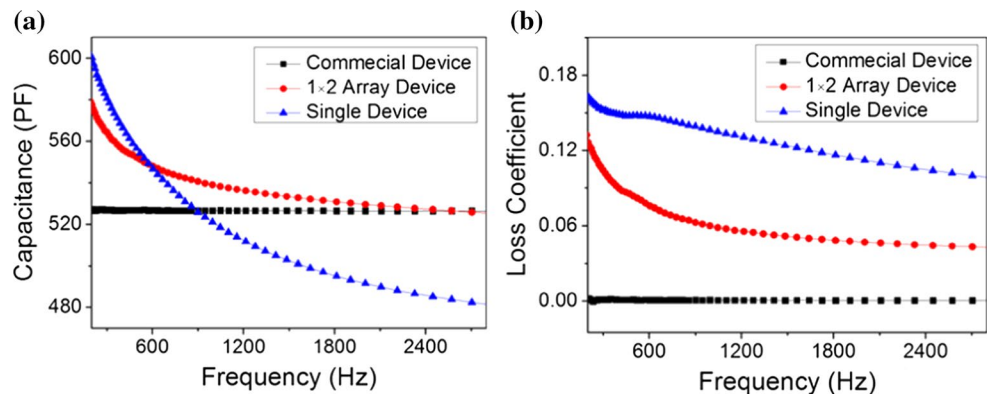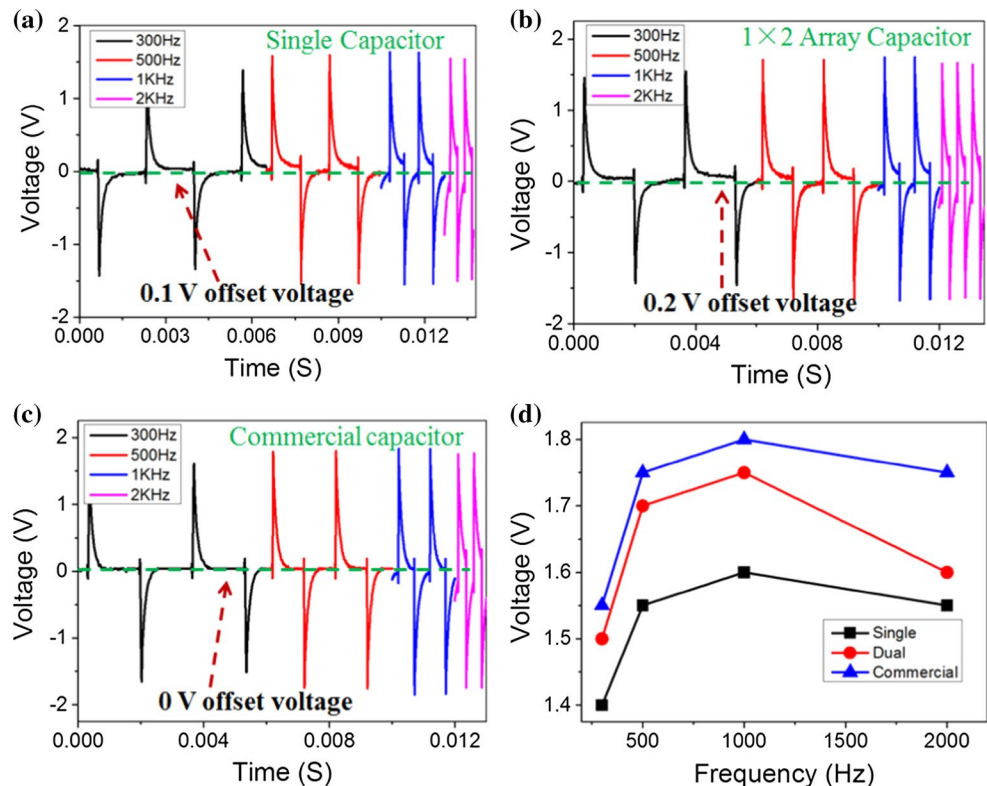

Fig. 4 Measured electrical performance of the variable capacitive high-pass filter: **a** results using single capacitor; **b** results using 1 × 2 array capacitor; **c** results using commercial static capacitor; **d** the peak output voltage with increasing frequency
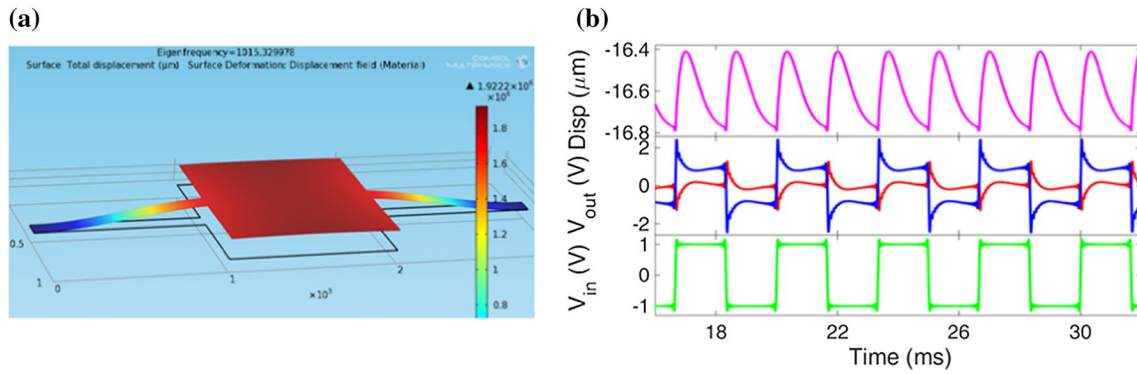
(a)

(b)

Fig. 5 Simulation results of the single variable capacitive filter: **a** FEM of the beam and plate; **b** numerical simulation results of the plate motion and the output voltage

Table 1 Simulation parameters of the fixed-end variable capacitive high-pass filter

System parameters	Symbols	Values and unit
Bottom air gap	d_0	0.5 mm
Movable plate thickness	h	5 μm
Movable plate area	A	1 mm^2
Constant permittivity	ε	210e-9
Damping ratio	δ	0.8
Silicon gap width	w_s	0.2 mm
Cantilever beam length	L_t	500 μm
Cantilever beam length	W	40 μm
Cantilever beam thickness	L_t	5 μm
Motioned capacitance	C_m	550 pF
Resistance	R_m	220 kΩ

5 Numerical simulation

The first mode of MEMS variable capacitor is shown in Fig. 5a and has been obtained from a finite element analysis (FEA) simulation performed with *COMSOL Multiphysics*. The simulation with approximately 16072 3D solid elements resulted in a 1015.3 Hz expected resonance frequency. The numerical simulation to the parameters such as displacement of the movable plate and the output voltage were shown in Fig. 5b. The parameters used in the computation are given in Table 1. The output voltage on the resistor and capacitor are the red curve and blue curve, respectively. When the MEMS variable capacitor is charging, the voltage across the capacitor increases but the output voltage across the resistor decreases. We found that the displacement of the movable plate was motioned around 16.6 μm position. We also found that the trends of the output voltage across the resistor with the numerical results are quite similar with experimental test results shown in Fig. 4a. Keep in mind

that we assumed the squeeze film air damping a constant coefficient in the numerical modeling.

6 Conclusion

In this study, we successfully fabricated a suspended fixed-end 5 μm thin SiO$_2$ film beam and plate using bulk silicon two-sided alignment micromachining technology. We have built a mathematical model which both includes a high-pass filter electrical system and variable capacitors driven by mechanical structural deformation. We found that the room temperature experiment of the designed MEMS high-pass filter can convert a rectangular wave input signal into high frequency spikes as its output. We also used both finite element calculating software *COMSOL* and numerical simulation *MATLAB* to evaluate the motion and the output voltage, and we demonstrated the room temperature measurement and the simulation modeling had a good agreement. We found that the parallel connection of the 1 × 2 array capacitors caused stronger asymmetric offset voltage electrical response performance than single capacitor due to the nonlinear dynamic of the variable electrostatic force with the motioned plate.

References

Baginsky IL, Kostsov EG, Kamishlov VF (2013) Two-capacitor electrostatic microgenerators. Engineering 05(11):9–18. doi:10.4236/eng.2013.511A002

Basu J, Bhattacharyya TK (2011) Microelectromechanical resonators for radio frequency communication applications. Microsyst Technol 17(10–11):187–218. doi:10.1007/s00542-011-1332-9

Bijari A, Keshmiri SH, Wanburee W, Sriphung CH, Phatthanakun R (2012) Design and fabrication of a narrow-bandwidth micromechanical ring filter using a novel process in UV-LIGA technology. Iran J Electr Electron Eng 8(4):280–289

Caruntu DI, Knecht MW (2015) Microelectromechanical systems cantilever resonators under soft alternating current voltage of frequency near natural frequency. J Dyn Syst Meas Control 137(4):041016:1–8. doi:10.1115/1.4028887

Chivukula VB, Rhoads J (2010) Microelectromechanical band-pass filters based on cyclic coupling architectures. J Sound Vib 329(20):4313–4332. doi:10.1016/j.jsv.2010.04.022

Dong L, Yu Q, Bao J, Tao J (2014) The slope effect of a capacitive resonator profile fabricated by a DRIE process on the performance of an MEMS disk resonator. J Micromech Microeng 24(10):105009:1–8. doi:10.1088/0960-1317/24/10/105009

Erbes DC, Yan A, Seshia A (2016) Design and implementation of a low-power hybrid capacitive MEMS oscillator. Microelectron J 56:1–9. doi:10.1016/j.mejo.2016.07.007

Galayko D, Basset P (2011) A general analytical tool for the design of vibration energy harvesters (VEHs) based on the mechanical impedance concept. IEEE Trans Circuits Syst 58(2):299–311. doi:10.1109/TCSI.2010.2072030

Hore S, Maity S, Sarma J, Choudhury A, Yadav G (2016) RF MEMS based band-pass filter for K-band applications. Adv Comput Commun Technol 452:369–375. doi:10.1007/978-981-10-1023-1_37

Kambali PN, Pandey AK (2016) Capacitance and force computation due to direct and fringing effects in MEMS/NEMS arrays. IEEE Sens J 16(2):375–382. doi:10.1109/jsen.2015.2480842

Lang LJ, Xia Y, Lim XH, Liu Y, Fang DM, Zhang HA (2011) Fabrication and characteristics of tunable bandPass filter using metal mumps technology. Nano/Micro Engineered and Molecular Systems (NEMS), 2011 IEEE International Conference. 20–23 February 2011, pp 249–253. doi:10.1109/NEMS.2011.6017341

Langfelder G, Frizzi T, Longoni A, Tocchio A, Manelli D, Lasalandra E (2011) Readout of MEMS capacitive sensors beyond the condition of pull-in instability. Sens Actuators A. doi:10.1016/j.sna.2011.02.003

Saha SC, Hanke U, Sagberg H, Fjeldly TA, Sather T (2011) Tunable band-pass filter using RF MEMS capacitance and transmission line. Prog Electromagn Res C 23:233–247

Shirazi FA, Velni JM, Grigoriadis KM (2011) An LPV design approach for voltage control of an electrostatic MEMS actuator. J Micromech Microelectromech Syst 2(1):302–311. doi:10.1109/JMEMS.2010.2090651

Tvedt LGW, Nguyen DS, Halvorsen E (2010) Nonlinear behavior of an electrostatic energy harvester under wide- and narrowband excitation. J Microelectricmech Syst 9(12):305–316. doi:10.1109/JMEMS.2009.2039017

Wang Z, Zhong SA, Ding Y, Wang X (2010) Design and implementation of a low-pass filter for microsensor signal processing. J Semicond 31(12):1–4. doi:10.1088/1674-4926/31/12/125002

Xu C, Cheng K (2015) A switched capacitor based AC/DC resonant converter for high frequency AC power generation. Energies 8(10):10842–10860. doi:10.3390/en81010842

Yang B, Lee C, Kotlanka RK, Xie J, Lim SP (2010) A MEMS rotary comb mechanism for harvesting the kinetic energy of planar vibrations. J Micromech Microeng 20(6):065017:1–11. doi:10.1088/0960-1317/20/6/065017

Zhang WM, Yan H, Peng ZK, Meng G (2014) Electrostatic pull-in instability in MEMS/NEMS: a review. Sens Actuators A. doi:10.1016/j.sna.2014.04.025

Zhang WM, Hu KM, Peng ZK, Meng G (2015) Tunable micro and nanomechanical resonators. Sens (Basel) 15(10):26478–26566. doi:10.3390/s151026478